THE ASTROPHYSICAL JOURNAL, 427:459–474, 1994 May 20

A CONVERGING FLUX MODEL OF AN X-RAY BRIGHT POINT AND AN ASSOCIATED CANCELING MAGNETIC FEATURE

E. R. PRIEST AND C. E. PARNELL
Mathematical Sciences Department, The University, St. Andrews, KY16 9SS, Scotland
AND
S. F. MARTIN
Big Bear Solar Observatory, Caltech, Pasadena, CA 91125
Received 1993 April 26; accepted 1993 November 18

ABSTRACT

X-ray bright points are an important part of the solar corona and therefore of the coronal heating problem. When it was first realized that bright points are always situated above opposite polarity magnetic fragments in the photosphere, it was natural to suggest that such fragments represent emerging flux and that an X-ray bright point is caused by reconnection of the emerging flux with an overlying coronal magnetic field. However, a recent important discovery at the Big Bear Solar Observatory is that the magnetic fragments of opposite polarity are usually not emerging but are instead coming together and disappearing and so are referred to as *canceling magnetic features*. Sometimes a tiny filament is observed to form and erupt at the same time.

A unified model is here proposed which explains these observational features and has several phases:

1. a *preinteraction phase*, in which two photospheric fragments are unconnected magnetically and begin to approach one another, until eventually oppositely directed fields from the fragments come into contact at a second-order null point;

2. an *interaction phase*, in which the null point becomes an X-point and rises into the corona; an X-ray bright point is created for typically 8 hr by coronal reconnection, driven by the continued approach of the photospheric sources; long hot loops and *Yohkoh* X-ray jets may be created by the reconnection, and rapid variability in bright point emission may be produced by an impulsive bursty regime of reconnection; the *explosive events* seen with HRTS may be produced as the X-point passes through the upper chromosphere;

3. a *cancellation phase*, in which a canceling magnetic feature is produced by photospheric reconnection as the fragments come into contact and decrease in strength; above the canceling fragments a small filament may form and erupt over typically an hour.

An important role is played by the *interaction distance* (d), which is proportional to the magnetic flux of the fragments and inversely proportional to the overlying magnetic field strength. It determines the fragment separation at which the interaction phase begins and the resulting maximum height of the reconnection point.

It is suggested that coronal reconnection driven by footpoint motion represents an *elementary heating event* that may be heating normal coronal loops and may be at the root of the nanoflare/microflare process. Bright points may well be at the large-scale end of a broad spectrum of events of the type modeled in this paper, which are heating the solar corona. At very small scales, such events in "furnaces" in the coronal hole network may even produce high-frequency waves that propagate out and drive the solar wind (Axford 1993).

Subject headings: MHD — Sun: corona — Sun: magnetic fields — Sun: X-rays, gamma rays

1. INTRODUCTION

X-ray bright points (BPs) are situated in the corona above pairs of opposite-polarity photospheric magnetic fragments. They were discovered by Vaiana et al. (1970) from rocket X-ray images, and their basic properties from *Skylab* images were studied by Golub et al. (1974, 1977) and Golub, Krieger, & Vaiana (1976a, b). They form as diffuse clouds which grow at 1 km s^{-1}, and then a bright core of width 3 Mm forms and later fades, followed by the fading of the diffuse cloud. At sunspot minimum they are more numerous and more uniformly distributed over the surface than during solar maximum, and 200 are seen to be present at any one time. The number as a function of their lifetime increases with decreasing lifetime.

Later, large numbers of *ephemeral active regions* (ERs) were discovered (Harvey & Martin 1973; Harvey, Harvey, & Martin 1975; Martin & Harvey 1979). They are small emerging magnetic dipoles with a flux of (2–3) $\times 10^{11}$ Wb (2–3 $\times 10^{19}$ Mx) and with more random orientations than for active regions. Also, it was discovered by Harvey et al. (1975) and Golub et al. (1989) that *helium 10830 dark points* (DP) are proxies for large BPs (the 30% largest). The lifetimes are 2–48 hr for BPs, a few to 48 hr for ERs and 10 minutes–24 hr for DPs. The sizes are typically 20 Mm for BPs (*Skylab*) or 6 × 9 Mm from Normal Incidence X-Ray Telescope (NIXT) with much less scatter (L. Golub, 1993 private communication), 30 Mm for ERs and 7–20 Mm for DPs, while the number born per day is estimated to be 1500 for BPs (Golub et al. 1974), 1200–1800 for DPs. (K. Harvey 1993 private communication), and 100 for ERs (Harvey & Martin 1973) from Kitt Peak magnetograms, although of course these numbers vary with the solar

cycle. A newer estimate for the number of ERs from the more sensitive Big Bear magnetograms in 1987 December (Webb et al. 1993) is 1200 per day, which would be expected to vary from roughly 600 at solar minimum to 2400 at solar maximum. A similar estimate by K. Harvey (1993, private communication) is 500–800 at solar minimum and 1200–2000 at solar maximum, depending on whether the mean lifetime is 8 hr or 5 hr.

As well as being a key part of the solar corona, bright points may eject mass into the solar wind since they are observed to lie at the base of polar plumes in coronal holes (Ahmad & Webb 1978; Bohlin et al. 1975). They are also often related to boundary changes of coronal holes, presumably by reconnection with the coronal hole magnetic field (Kahler & Moses 1990).

It was natural to assume that BPs are always regions of newly emerging flux, but this suggestion is not tenable because the number of BPs is observed to be out of phase with the solar cycle (Davis, Golub, & Krieger 1977; Golub, Davis, & Krieger 1979), while the number of ERs is in phase (Harvey et al. 1975; Martin & Harvey 1979): it doubles from solar minimum (when they are almost uniformly distributed over the solar surface) to solar maximum (when they have peaks at latitudes $\pm 30°$ and $\pm 50°$). This major puzzle was solved in two key papers by K. Harvey (1984, 1985), who showed that, although one-third of the DPs and (therefore presumably BPs) overlie emerging ERs, two-thirds of them lie above so-called *canceling magnetic features* (CMFs). These are opposite polarity magnetic fragments that are seen in the Big Bear video magnetograms to be approaching one another and disappearing (Martin et al. 1984; Martin, Livi, & Wang 1985; Zirin 1985; Martin 1984, 1986, 1988, 1990a, b; Martin et al. 1985; Livi, Wang, & Martin 1985, 1989). The term "cancellation" is an observational one and is defined as the mutual disappearance of observed magnetic flux of opposite polarity at a common boundary as seen in magnetograms of the line-of-sight component. CMFs have several properties: the fragments have fluxes and fields greater than 10^{17} Mx and 20 G, respectively; the fragments are approaching one another and have an increasing magnetic gradient between them; and there is a loss of flux in both fragments during cancellation. There are 3 or 4 times as many CMFs present as BPs (Webb et al. 1993) and those CMFs that are associated with BPs tend to be the strongest. K. Harvey suggested that most BPs are due to chance encounters of opposite polarity fragments in the network or of emerging flux with opposite polarity network. She pointed out that such cancellations should depend on the amount of mixed-polarity areas, which decreases by a factor of 6 from 95% at solar minimum (1976) to 14% at solar maximum (1979–1980), while the number of BPs also decreases by a factor 6 from 90 to 14. This explains the anticorrelation of the BPs with the solar cycle. An example of a BP and a CMF is shown in Figure 1 (Plate 9).

Many time variations are observed in BPs. Golub et al. (1974) report that 5%–10% of them flare with their intensity increasing by a factor of 10 (see also Moore et al. 1977, Sheeley & Golub 1979, Habbal & Withbroe 1981). More recently a study of Strong et al. (1992) from *Yohkoh* has shown that BPs fluctuate in intensity by 30%–200% over timescales from a few minutes to hours. Also, they find that BP flares involve neighboring loop brightenings at CMFs, with the intensity increasing by a factor of 10 to 100 and the brightening occurring at speeds of up to 1100 km s^{-1}. Furthermore, radio BPs have been described by Habbal et al. (1986), Fu, Kundu, & Schmahl (1987), Kundu, Schmahl, & Fu (1988), and Nitta et al. (1992) who find BP temperatures of $(1.4–2.9) \times 10^6$ K.

It would be interesting to know whether there is a relation between BPs and the transition region brightenings in C IV from the UVSP instrument on *SMM* (Porter et al. 1987; Habbal & Withbroe 1981) and the HRTS explosive events in C IV (Brueckner & Bartoe 1983; Dere et al. 1991), which have timescales of 20 s, velocities usually of 10–20 km s^{-1}, sizes of 1 Mm, and densities of 10^{16} m^{-3}. More recently, Dere (1993) has reviewed the properties of explosive events. They are at an altitude of 1–2 Mm (i.e., below the quiet-Sun transition region) and so probably represent heating events from 10^4 K to 10^5 K. Velocities may be up to 100 km s^{-1} or more with lifetimes of 60 s: the velocities may be asymmetric but there is no sign of motion along the slit, and so the events are likely to represent the sites of acceleration. The densities are about 7×10^{16} m^{-3} by comparison with the quiet-Sun density of 10^{16} m^{-3}. Most of the explosive events are situated at the network; some are associated with cancelling magnetic features and occur repetitively, but many have no magnetic signature, perhaps because they are below current observational thresholds.

Thus, some BPs (typically one-third) are probably caused by emerging flux and may be explained in terms of reconnection between newly emerging flux and overlying field, as in the emerging flux model (Heyvaerts, Priest, & Rust 1977) and as modeled analytically by Tur & Priest (1976) and numerically by Forbes & Priest (1984), Shibata et al. (1992a, b), Yokoyama & Shibata (1993). However, most BPs are associated instead with CMFs; and many of the ER associations may also involve cancellation: for instance, Webb et al. (1993) find that sometimes a BP occurs above an ER interacting with an intracell element. So what is happening during a cancellation? The natural explanation is at first sight that they represent regions of *simple submergence*, where a flux tube is descending through the photosphere, and another possibility is that they are instead regions of *reconnection submergence* where field lines are first reconnecting in the corona and then submerging through the photosphere. This idea was first proposed in cartoon form by Priest (1987) and Zwaan (1987), but the present model differs from both possibilities and is worked out in much more detail, both physically and mathematically.

The difficulties with simple submergence are that it gives no explanation for the overlying coronal energy release (the X-ray brightening) and the fact that the brightening starts before the cancellation. Also, although emerging flux with separating magnetic fragments in the photosphere is observed, such fragments are never observed to reverse direction and cancel. The evidence to date is that the fragments which cancel are initially very widely separated and therefore rarely connected magnetically. So we need to include the effect of the ambient magnetic field. The main difficulty with reconnection submergence is that Hα fibrils are rarely observed to be joining the two magnetic fragments. We would therefore like to propose here a third possibility, a *Converging Flux Model* which accounts for many diverse observations in a unified and natural manner.

In the next section we describe the basic physical model and explain how it accounts for the main observational features. Section 3 gives some theoretical details of the model, together with a calculation of the free magnetic energy which is released to give the X-ray bright point. It also describes a dynamic current sheet model of energy release. Section 4 discusses other

1994ApJ...427..459P

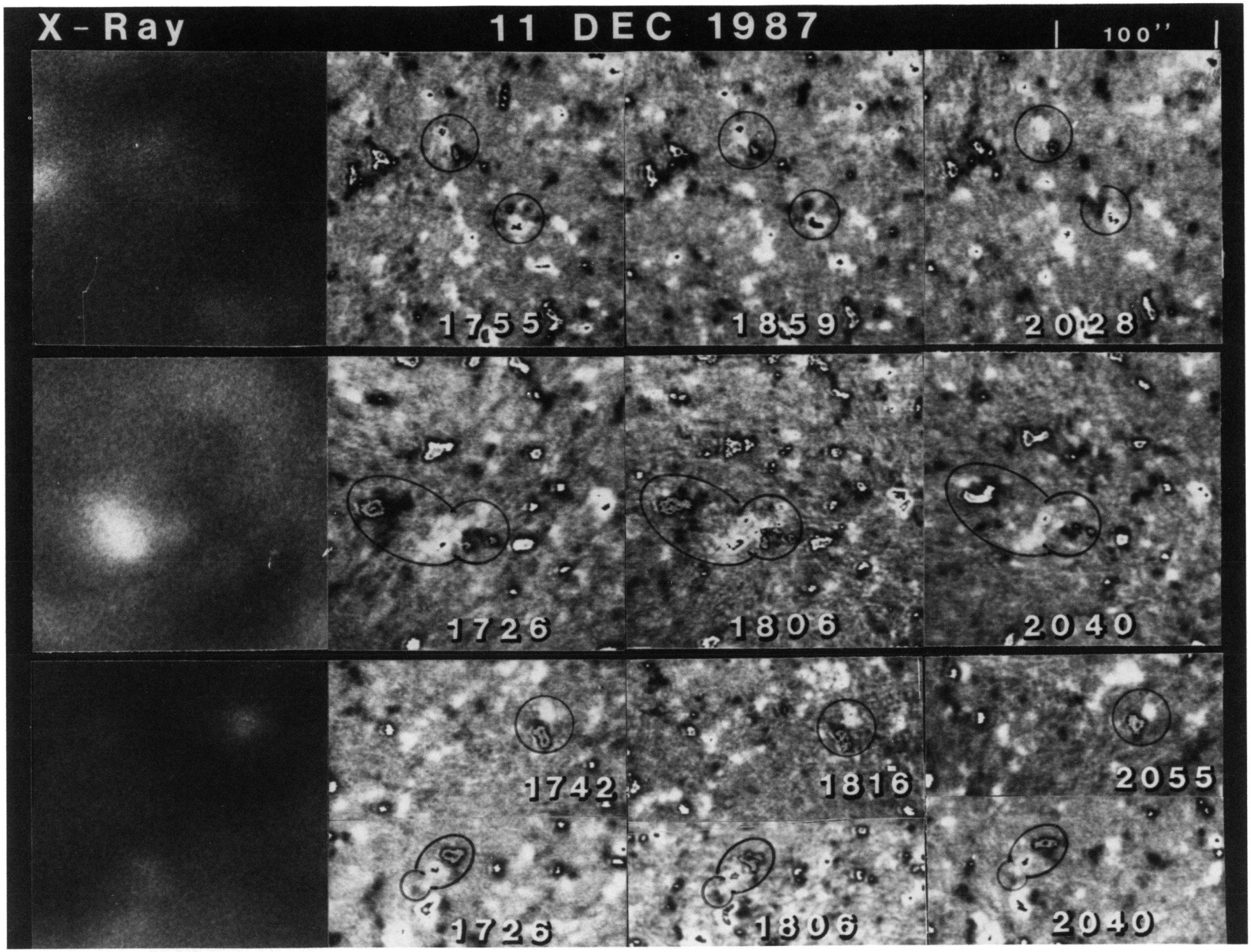

FIG. 1.—Examples of (*left*) bright points in soft X-rays from the AS&E rocket flight at 18.30 on 1987 December 11 (courtesy D. Moses and D. Webb) and (*right*) canceling magnetic features in photospheric video magnetograms from Big Bear Solar Observatory. The features within the ovals are ephemeral active regions (ER); the circles enclose apparent bipoles that are slowly canceling (reducing in magnetic flux). The positive polarity pole of each ER is also a canceling magnetic feature where neighboring flux has been encountered. White is positive polarity and black is negative, except within the contours where stronger flux of the same polarity is indicated by nested dark and light contours.

PRIEST, PARNELL, & MARTIN (see 427, 460)

PLATE 9

qualitative aspects of the model and makes suggestions for future observational work, and the final section presents the conclusions.

2. BASIC MODEL

2.1. *Key Observational Constraints on a Model*

There are several features of the observations of most bright points which need to be explained:

1. *Preinteraction Phase.*—Photospheric magnetic field patches of opposite polarity slowly approach one another;

(1a) chromospheric fibril-like features are rarely observed to join the opposite fragments (Martin et al. 1985; Martin 1988), although see the comments in § 4.2;

(1b) as the fragments approach, the chromospheric fibrils turn away from one another (Martin 1986), although several other scenarios are possible, depending on the details of the surrounding fields which vary from one BP to another;

(1c) the typical diameter of a magnetic fragment is 5 Mm, and its typical speed is 0.5 km s^{-1}.

2. *Interaction Phase.*—Energy is released in the corona as a BP and a DP;

(2a) the DP and BP begin before the fragments come into contact and cancel (Harvey 1985; Webb et al. 1993);

(2b) the duration of the BP is 2–48 hr, with a mean value of 8 hr (Golub et al. 1974) or, from more recent *Yohkoh* Soft X-Ray Telescope (SXT) images, 2 minutes–5 days, with an average of 12 hr (Harvey et al. 1992);

(2c) often long hot loops and X-ray jets are observed in association with flaring BPs by the SXT on the *Yohkoh* satellite (Shibata et al. 1992a, b; Uchida 1992; Tsuneta 1992; Strong et al. 1992): such a frequent connection of BPs with distant locations was one of the many surprises revealed recently by *Yohkoh*; the jets have sizes 5–400 Mm and velocities of 30–300 km s^{-1}.

3. *Cancellation Phase.*—The photospheric fragments slowly cancel (CMF): present observations show that about 20% of CMFs are associated with BPs, while 72% of BPs are associated with CMFs and 88% with converging magnetic features (Webb et al. 1993), although these percentages may vary with the solar cycle.

(3a) Sometimes, well after cancellation has begun, a tiny filament forms and erupts (Hermans & Martin 1986) and/or a small chromospheric brightening (flare) is seen. Most of the tiny filaments form, expand, and erupt during the cancellation process in tens of minutes to a few hours. Many seem like one continuous event, as if they are preparing to erupt as they form. With present observations, we estimate that 10% of CMFs have associated tiny erupting filaments, but there are not yet any studies that relate BPs with them. Also, many ejecta associated with DP and BP flares are like surges or jets (K. Harvey, 1993 private communication).

(3b) The cancellation phase overlaps with the interaction phase (Webb et al. 1993).

(3c) There is a continuous range in the fluxes of the fragments and the duration of the cancellation, but typical values from current observations are as follows. For intracell/intracell or intracell/network cancellations, the flux in each pole is about 10^{18} Mx, and its size with the present resolution is 1–5 Mm, while the duration and speed of cancellation are 1–5 hr and 0.3 km s^{-1}. For network/network cancellations, the flux is 10^{18}–10^{19} Mx, and the size is 1–10 Mm, while the duration is 1–36 hr and the speed is 0.1–0.3 km s^{-1}. For ephemeral region/network or ephemeral region/intracell cancellations the flux is 10^{18}–5×10^{19} Mx, while the duration and speed are 1–36 hr and 0.1–0.3 km s^{-1}, although the mean lifetime is smaller and the mean speed higher than for the network/network case. Typical field strengths at a resolution of 2″–3″ (Big Bear Solar Observatory) are 10 G for intracell features (Zirin 1987), 100–200 G for quiet-Sun network, 100–400 G for active region network (although a fully resolved upper limit would probably be 1–2 kG [Stenflo 1973; Keller 1992]), and 100–600 G for ER (Chou & Wang 1987).

2.2. *Physical Stages of a Converging Flux Model*

Before the key observations and analysis of canceling magnetic features were made at Big Bear Solar Observatory, the standard explanation of X-ray bright points was in terms of emerging flux. But this is clearly inoperative for the majority of bright points with the features outlined above. We therefore aim so set up an alternative model in which the magnetic fragments are initially unconnected and in which the bright point is created by coronal reconnection, while the canceling magnetic feature is produced by photospheric reconnection.

The basic Converging Flux Model that we would like to propose is shown in Figure 2. Of course, there may be a wide variety of different magnetic configurations between and around actual BPs and CMFs which in detail may appear to be rather different from Figure 2, but following the usual philosophy of mathematical modeling, we are suggesting that the key physical processes which are central to most BPs are well represented by the present model. It has several phases.

(i) Oppositely directed magnetic fragments are far apart and unconnected but are approaching one another in a *preinteraction phase* (observation 1). Between them the overlying field between the fragments has a component out of the plane of Figure 2, which is in agreement with the observed usual lack of connecting fibrils (observation 1a). As the fragments approach, the overlying field lines tilt away from one another (observation 1b).

(ii) Eventually, the fragments become so close that an X-point (or in three dimensions, a separator) forms between them in the photosphere and the *interaction phase* begins.

(iii) The field lines from the two fragments can then interact and reconnect at the X-point, which rises from the photosphere into the corona. The magnetic energy that is liberated in the coronal reconnection process shows up as an X-ray bright point (observation 2), well before the magnetic fragments appear to touch one another in the photosphere (observation 2a).

(iv) As the fragments approach, the reconnection and BP continue for typically 8 hr. Prior to reconnection forming the BP, the network is already connected to distant magnetic fields of opposite polarity. During creation of the BP, the reconnection process and its associated evaporation injects hot plasma into these field lines to create X-ray jets and very long hot loops (observation 2c—see Shibata et al. 1992a, b, who suggested that jets are produced by evaporation driven by reconnection between emerging flux and a preexisting coronal field). In the simplest (symmetric) version of the model the hot loops extend out equally to left and right in Figure 2*d*, but normally there is a large asymmetry in the two interacting fragments (Fig. 9*b*–9*d*), and so the hot loop and X-ray jet go out preferentially in one direction (see also § 4.5). The spatial structure of the bright point and its environment consists of a bright core

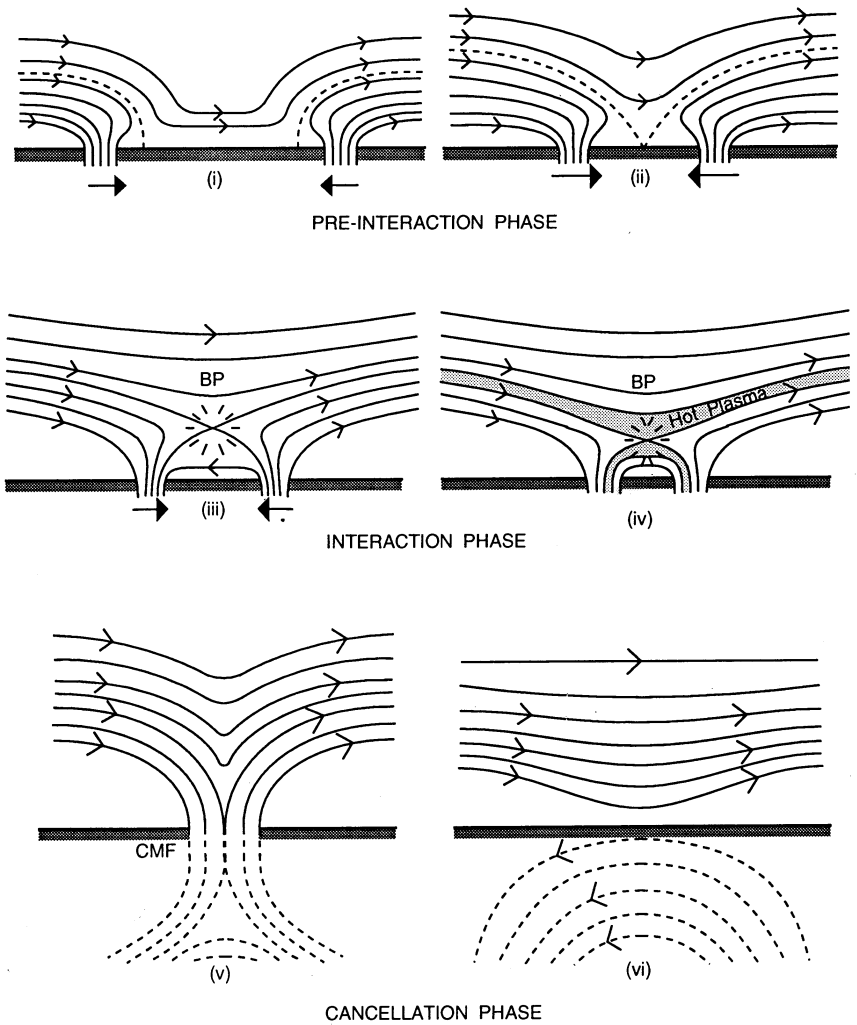

FIG. 2.—Stages in the approach and interaction of two equal and opposite magnetic fragments, showing the projection of the magnetic field lines in the plane of approach (*solid curves*) and the separatrix field lines (*dashed curves*). Shown are (*a*)–(*b*) the pre-interaction phase; (*c*)–(*d*) the interaction phase, during which an X-ray bright point (BP) is created by coronal reconnection; (*e*) the cancellation phase, during which a cancelling magnetic feature (CMF) is produced by photospheric reconnection, and sometimes a tiny filament forms and erupts (see Fig. 3); and (*f*) the final state with magnetic flux above (*solid curves*) and below (*dashed curves*) the photosphere.

near the X-point, together with the hot looplike reconnected field lines below the X-point and sometimes long hot overlying loops. As the fragments approach, so the X-point and its underlying loops first rise and then lower (Fig. 5*b*), although the amount by which the released energy spreads from the release site and the cooling rate may both also vary. The rapid variability that is sometimes seen in BP emission may be created when reconnection enters the impulsive bursty regime (Priest 1986).

(v) The fragments come into contact and the *cancellation phase* begins by photospheric reconnection (observation 3). Since the fragments are being pushed toward one another, presumably by a photospheric or subphotospheric flow, reconnection is likely to be by the *flux pile-up regime* (Priest & Forbes 1986), which is consistent with an observed increase of field gradient near the cancellation (Martin 1986) and the occurrence of reconnection at the photosphere. Also, Wang & Shi (1993) have recently shown for some active region cancellations that the evolution of the transverse field is consistent with photospheric reconnection. The reconnected flux is ejected upward toward the corona and downward below the photosphere. The bright point continues until at least the first part of the cancellation phase. A tiny filament sometimes forms and erupts. The field may be inclined at any angle to the plane of Figure 2, and, if there is a large component out of the plane, then cancellation naturally produces a filament, since it creates long field lines (Fig. 3).

(vi) The cancellation by photospheric reconnection continues and the fluxes decrease until either the approach of the fragments ceases or one or both of the fragments have completely canceled. In the case when the initial fragments had equal but opposite magnetic flux, the final state is a horizontal flux tube above the photosphere and another flux tube that remains below the photosphere.

3. MODEL OF SIMPLE INTERACTION

A simple mathematical model of the *preinteraction* and *interaction phases* of the process ([i]–[iv] in Fig. 2), during which the X-ray bright point is created, may be set up by representing the two oppositely directed magnetic fragments by equal but

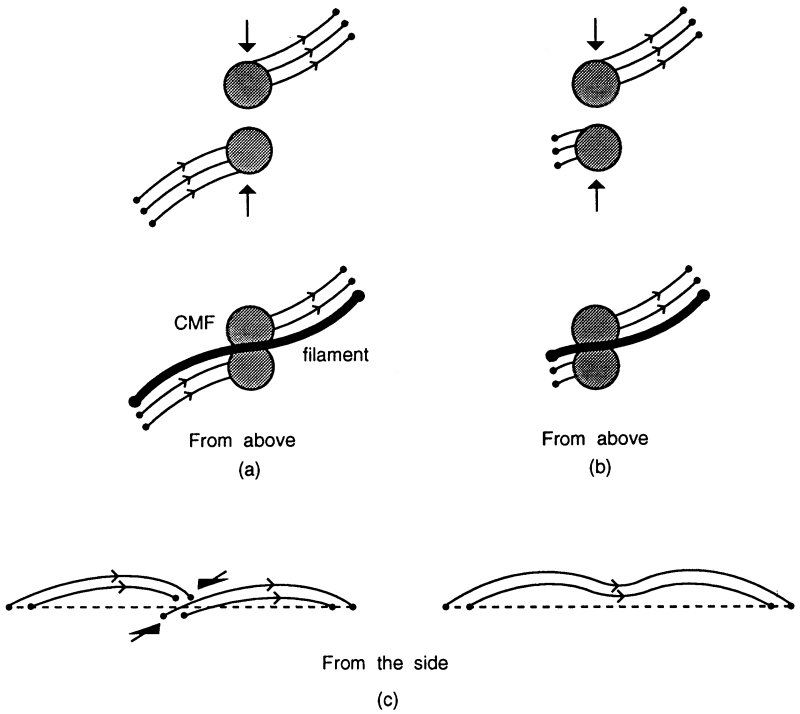

FIG. 3.—Tiny filament formation and eruption above the approaching fragments in Fig. 2(*e*): (*a*) or (*b*) from above in the case when the field component out of the plane of Fig. 2 dominates; (*c*) from the side.

opposite magnetic poles on the photospheric boundary $y = 0$. Although in classical electromagnetism magnetic poles may not exist in free space, it is, of course, allowable to represent a source of magnetic flux passing through a boundary by a pole placed on the boundary creating flux on one side of the boundary.

If there were no other sources or sinks present, the resulting potential field would have all the field lines from one pole ending on the other pole. A key point of our model, however, is that initially the magnetic fragments are unconnected. We assume, therefore, that initially, when the poles are a distance $2a$, say, apart (Fig. 4[i]), they are connected to a field which is uniform at large distances (infinity) and remains constant in time during the subsequent evolution. The poles then approach one another slowly at a speed much less than the coronal Alfvén speed (by a factor of typically a 100–1000) in such a manner that the overlying magnetic field evolves through a series of configurations that are piecewise potential.

Initially, the two poles are so far apart that the overlying field dips down between them to fill a channel of width $2b$, say, separating the flux from the poles. As the poles approach, the channel narrows until eventually when the pole half-separation is d, say (we refer to d as the *interaction distance*), a null point is formed at the origin (Fig. 4[ii]). After this stage, if no reconnection occurs so that the topology is preserved, a vertical current sheet will be created stretching up a height h, say, when the fragment separation is $2a$ (Fig. 4[iii]). The magnetic energy then exceeds that of a purely potential field by an amount that can be released by reconnection to give an X-ray bright point and the potential configuration shown in Figure 4(iv).

In practice, reconnection will continuously take place as the fragments approach one another and the magnetic energy is continuously converted into the heat of the BP. Nevertheless, the thought experiment of supposing the current sheet is first created (Fig. 4[iii]) and then dissipated is useful, since it enables us to estimate roughly how much energy is released.

The magnetic field components (B_x, B_y) due to a line source at a point $z = x_0$ on the x-axis are given in compact form by

$$B_y + iB_x = \frac{iq}{\pi(z - x_0)}, \tag{3.1}$$

in terms of the complex variable $z = x + iy$, where q is the magnetic flux per unit length perpendicular to the xy-plane that comes from the source into the upper-half plane ($y > 0$). We therefore suppose the upper-half plane represents the corona and the x-axis ($y = 0$) the photospheric boundary. We model two magnetic fragments of equal strength but opposite polarity by sources of flux $+f$ and $-f$ located at $z = a$ and $z = -a$, respectively. Adding also a uniform horizontal field of strength B_0, the resulting magnetic field is

$$B_y + iB_x = \frac{if/\pi}{z - a} - \frac{if/\pi}{z + a} + iB_0, \tag{3.2}$$

or

$$B_y + iB_x = iB_0 \frac{z^2 - b^2}{z^2 - a^2}, \tag{3.3}$$

where

$$b^2 = a^2 - \frac{2af}{\pi B_0}. \tag{3.4}$$

The form of the field (eq. [3.3]) is sketched in Figure 4(i) and the way the half-width (b) of the channel between the fragments varies with the fragment location (a) according to equation

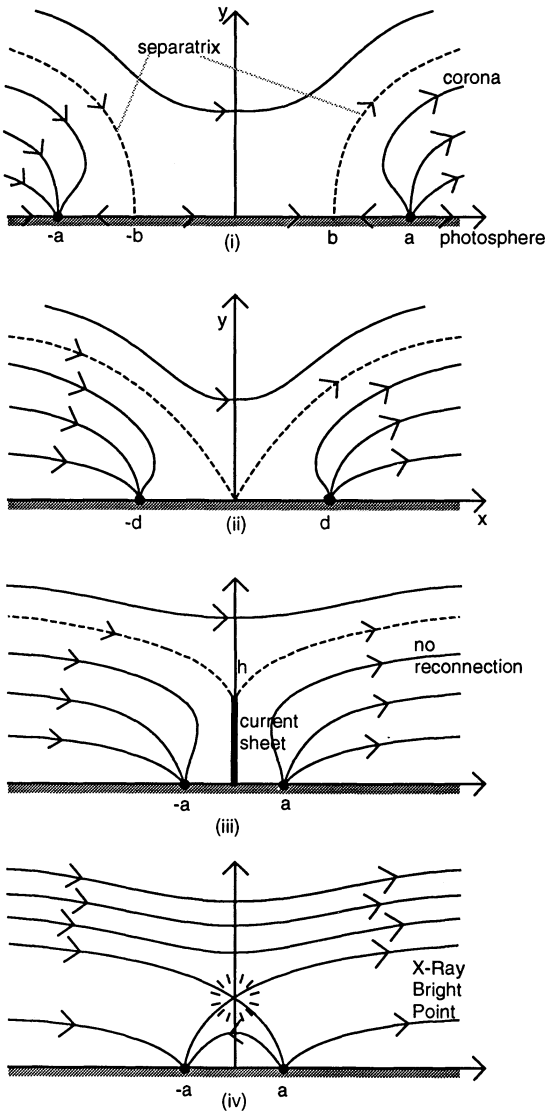

FIG. 4.—A model of (i)–(ii) the pre-interaction phase and (iv) the interaction phase when the magnetic fragments are represented as poles at distances $\pm a$ along the x-axis. The label b is the half-width of the preinteraction channel, and h is the height of the current sheet when no reconnection takes place.

(3.4) is sketched in Figure 5*a*. The separatrices (separating the overlying flux from the flux of the fragments) intersect the photosphere at right angles at the points $\pm b$. The field on the y-axis is

$$B_x = B_0 \frac{y^2 + b^2}{y^2 + a^2},$$

and so the magnetic flux crossing the positive y-axis (up to some large finite height H much larger than a) is

$$\int_0^H B_0 \frac{y^2 + b^2}{y^2 + a^2}\, dy = \int_0^H B_0\, dy + \frac{B_0 \pi}{2a}(b^2 - a^2).$$

The first term on the right represents the flux of the ambient uniform field and the second may be rewritten, after substituting for b^2 from equation (3.4), simply as f. Thus, the flux crossing the y-axis remains constant as the sources approach one another and a decreases.

At large separation distances $[a \gg 2f/(\pi B_0)]$ $b \approx a$, but when

$$a = d \equiv \frac{2f}{\pi B_0}, \tag{3.5}$$

it can be seen from equation (3.4) that $b = 0$, and so the channel is squeezed from the photosphere and a null point forms at the origin (Fig. 4 [ii]). Thus the form (eq. [3.3]) is valid for half-separations (a) of the fragments in excess of the interaction distance (d). According to equation (3.5), the minimum separation ($2d$) for the existence of a channel in the photosphere is proportional to the fragment flux (f) and inversely proportional to the ambient field strength (B_0).

When $a = d$ (Fig. 4[ii]), b vanishes and so the field (eq. [3.3]) becomes

$$B_y + iB_x = iB_0 \frac{z^2}{z^2 - d^2}. \tag{3.6}$$

Thus, along the y-axis $B_x = B_0 y^2/(y^2 + d^2)$, while along the x-axis $B_x = B_0 x^2/(x^2 - d^2)$. Near the origin

$$B_y + iB_x \approx -iB_0 \frac{z^2}{d^2}, \tag{3.7}$$

and so

$$B_x = \frac{B_0}{d^2}(-x^2 + y^2), \quad B_y = \frac{2B_0}{d^2} xy.$$

In other words, the origin is a second-order null point with flux function

$$A = \frac{B_0}{d^2}\left(x^2 y - \frac{1}{3} y^3\right)$$

and field lines given by

$$x^2 = \frac{y^3 - C^3}{3y}, \tag{3.8}$$

where C is a constant. The separatrices are thus the positive and negative x-axis and the two field lines inclined at $\pi/3$ to the x-axis.

When the fragments are so close that $a < d$, magnetic reconnection is driven at the null point, which rises higher into the corona, the liberated magnetic energy creating the X-ray bright point. Describing the reconnection fully would need a numerical experiment (e.g., Biskamp 1986; Forbes & Priest 1987; Priest & Lee 1990; Scholer 1989; Lee & Fu 1986; Priest & Forbes 1992) and would involve shock waves and time-dependent effects.

However, a simple approximate treatment is to assume a slow evolution through a series of potential states given by equation (3.2), namely,

$$B_y + iB_x = iB_0 \frac{z^2 + c^2}{z^2 - a^2}, \tag{3.9}$$

where

$$c^2 = a(d - a) = \tfrac{1}{4}d^2 - (\tfrac{1}{2}d - a)^2. \tag{3.10}$$

These states possess an X-point at $z = ic$ on the y-axis above the photosphere (Fig. 4[iv]), and the variation of c with a for

$0 \leq a \leq d$ is shown in Figure 5*b*. As the fragments approach one another, so the height (c) of the reconnection point increases to a maximum of $\frac{1}{2}d$ when $a = \frac{1}{2}d$, and then it decreases toward zero as a tends to zero. The speed of rise ($\dot{c}$) of the X-point for a given speed of approach ($-\dot{a}$) of the fragments is given by differentiating equation (3.10) with respect to time as

$$\dot{c} = \frac{d - 2a}{2a(d - a)}\,\dot{a} \tag{3.11}$$

and is plotted in Figure 5*c*. Clearly, the speeds of rise and ascent tend to infinity as a approaches d and 0, respectively.

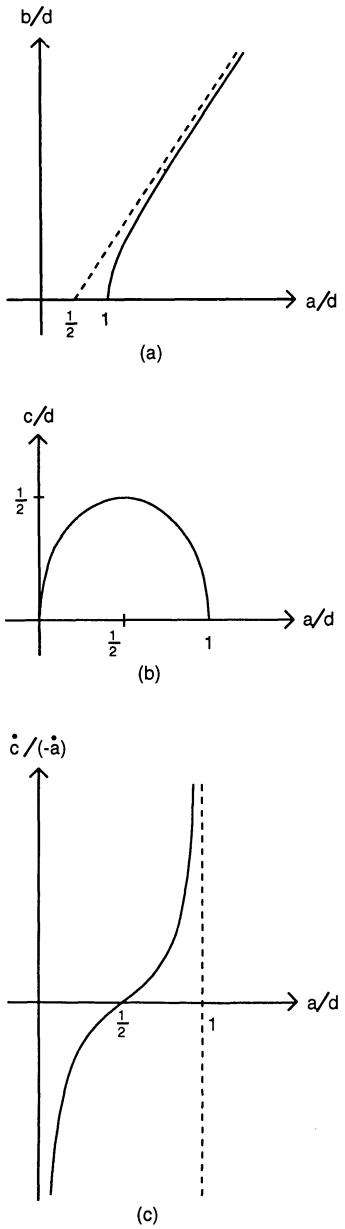

FIG. 5.—As a function of the half-separation distance, a, of the two magnetic fragments in terms of the interaction distance, d, we plot: (*a*) the preinteraction channel half-width, b, when $a \geq d$; (*b*) the height, c, of the X-point when $a \leq d$; (*c*) the rise speed, $\dot{c}$, of the X-point in terms of the speed of approach, $-\dot{a}$.

When the fragments are very close together, an alternative way of modeling the cancellation phase without taking account of the finite dimension of the fragments is to regard them as a dipole of strength D, say, in the uniform field B_0. The resulting field is

$$B_y + iB_x = \frac{iD}{z^2} + iB_0\,,$$

which has an X-point above the photosphere on the y-axis at a height

$$C = \left(\frac{D}{B_0}\right)^{1/2}.$$

Thus, as the fragments cancel, the strength D decreases to zero, and so the X-point moves down to the photosphere.

The above solution (eq. [3.9]) is valid in the limit when the speed of approach tends to zero and when one has vacuum reconnection. Another limit of interest is when there is no reconnection at all and again the fragments are approaching at a rate much smaller than the Alfvén speed. Thus, again the field passes through a series of potential configurations, but now the topology is preserved, and a current sheet of height h, say, must grow along the y-axis from the null point (Fig. 4[iii]). The resulting magnetic field may be represented by

$$B_y + iB_x = \frac{iB_0(z^2 + h^2)^{1/2}z}{(z^2 - a^2)}\,, \tag{3.12}$$

which has several useful properties that are required:

(1) at large distances ($z \gg a$) as $z \to \infty$, $B_y + iB_x \to iB_0$, and so the field approaches a uniform horizontal field of strength B_0;

(2) there is a cut in the upper-half complex plane stretching along the y-axis from the origin to $z = ih$:

(3) near $z = a$, the field behaves like

$$B_y + iB_x \approx \frac{iB_0(a^2 + h^2)^{1/2}}{2(z - a)}\,,$$

which is of the required form provided

$$\tfrac{1}{2}iB_0(a^2 + h^2)^{1/2} = if/\pi\,,$$

or

$$h^2 = d^2 - a^2\,. \tag{3.13}$$

According to equation (3.13), as the magnetic sources come closer and a decreases from d to zero, so the height (h) of the current sheet increases from zero to d (Fig. 6*a*). By differentiating equation (3.13) with respect to time, the rate ($\dot{h}$) at which the top of the current sheet is rising may be found in terms of the speed of approach ($-\dot{a}$) to be

$$\dot{h} = \frac{a}{d^2 - a^2}\,(-\dot{a})\,. \tag{3.14}$$

If the speed of approach is constant, the speed of rise is initially infinite when $a = d$ and then decreases monotonically toward zero as the fragments come closer (Fig. 6*b*).

The behavior of the magnetic field on the axes may be found from the solution (3.12). Near the origin

$$B_y + iB_x \approx \mp\frac{iB_0 h}{a^2}\,z\,, \tag{3.15}$$

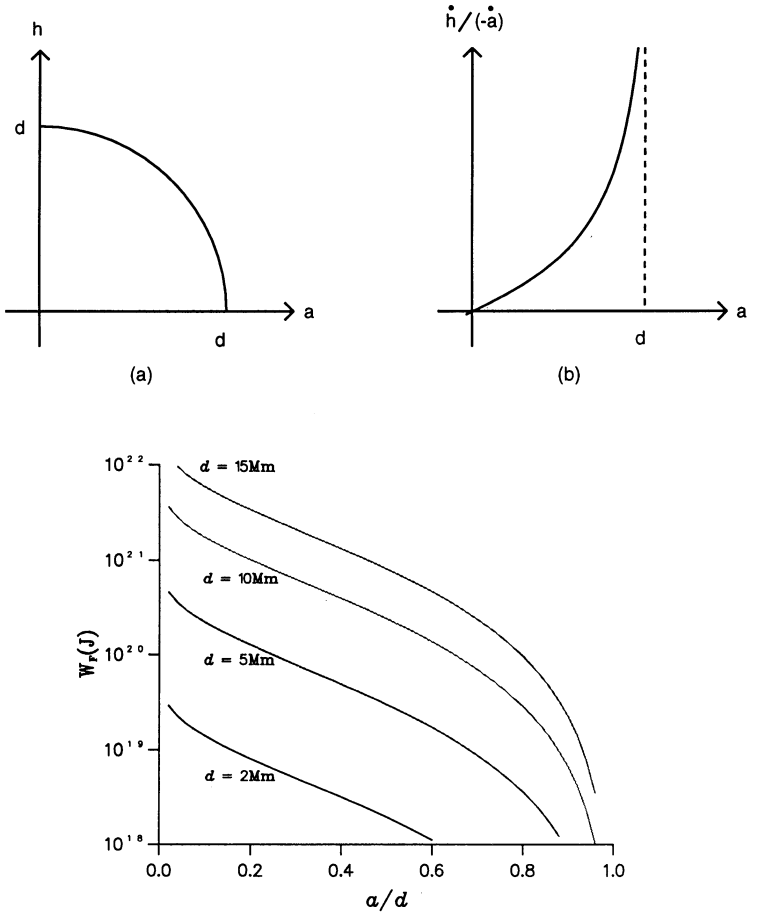

FIG. 6.—(*a*) The height, h, of the top of the current sheet and (*b*) its speed of rise, $\dot{h}$, as functions of the half-distance, a, between the fragments. (*c*) The free energy (W_f) in joules (1 J = 10^7 ergs) as a function of a for different values of the interaction distance, d, when the ambient field B_0 is 10 G.

where the negative and positive signs refer to $x > 0$ and $x < 0$, respectively, so $B_x \geq 0$ and the origin is a null point with a current sheet stretching up the y-axis. On the y-axis, for $y < h$, B_x vanishes and

$$B_y = \pm B_0 \frac{(h^2 - y^2)^{1/2} y}{y^2 + a^2}, \tag{3.16}$$

where the positive and negative signs correspond to locations to the right and to the left of the sheet, respectively. Thus, the field strength increases from zero to a maximum of $B_0(d^2 - a^2)/(2ad)$ at $y^2 = a^2(d^2 - a^2)/(d^2 + a^2)$ and then decreases to zero at the top ($y = h$) of the sheet. For $y > h$, B_y vanishes on the y-axis and

$$B_x = B_0 \frac{(y^2 - h^2)^{1/2} y}{y^2 + a^2}. \tag{3.17}$$

which increases monotonically from zero at $y = h$ to B_0 at infinity.

In the above calculation the magnetic flux above the sheet is conserved during the approach of the sources. The initial value when $a = d$ is, as before,

$$\int_0^H B_0 \, dy - f.$$

When the current sheet is present, the flux is

$$\int_h^H (B_x)_{x=0} \, dy = \int_h^H \frac{B_0(y^2 - h^2)^{1/2} y}{y^2 + a^2} \, dy,$$

which, by changing the variable to $Y^2 = y^2 - h^2$, gives the same result.

What is the appropriate value for the interaction distance (d) for flux interaction on the Sun? The value (eq. [3.5]) refers to our model of two-dimensional sources, and so we need to estimate the corresponding interaction distance (d^*) for three-dimensional sources. In such a case the magnetic field a distance d^* from a pole of half-flux f is $f/(2\pi d^{*2})$ and so, as in the calculation of equation (3.5), equating this to one-half the ambient field strength (B_0) gives

$$d^* = \left(\frac{f}{\pi B_0}\right)^{1/2}.$$

Now, the flux of intracell features, network features, and ephemeral region poles is typically 10^{18} Mx, 10^{18}–10^{19} Mx, and 10^{18}–5×10^{19} Mx, respectively, and so, when $B_0 = 10$ G, say, this gives values for d^* of 2 Mm, 2–5 Mm, and 2–12 Mm, respectively. For $B_0 = 5$ G, say, these values are increased by $\sqrt{2}$. These are consistent with the observation of Webb et al. (1993), who found one example where the opposite polarity features are as much as 19 Mm apart.

3.1. *Free Energy*

An upper limit to and a rough estimate of the energy released in the bright point may be obtained by finding the free energy stored in excess of potential in the field (eq. [3.12]) that includes the current sheet, i.e., by subtracting its energy from that of the potential solution (3.9). Low & Hu (1983) have developed an elegant method for finding the excess energy stored in a current sheet between approaching dipoles, and so we adopt the same basic approach as them, as follows.

If W is the magnetic energy of the magnetic field containing the current sheet, then, after writing the magnetic field ($\boldsymbol{B}$) in terms of the vector potential ($\boldsymbol{B} = \nabla \times \boldsymbol{A}$) and using standard vector identities, we obtain

$$2\mu W = \int B^2 dV = \int \boldsymbol{B} \cdot \nabla \times \boldsymbol{A}\, dV$$
$$= \int \boldsymbol{A} \cdot \nabla \times \boldsymbol{B} + \nabla \cdot (\boldsymbol{A} \times \boldsymbol{B})\, dV \qquad (3.18)$$

or, using Ampère's Law and the Gauss divergence theorem,

$$2\mu W = \int \mu \boldsymbol{A} \cdot \boldsymbol{j} dV + \int \boldsymbol{A} \times \boldsymbol{B} \cdot d\boldsymbol{S} . \qquad (3.19)$$

In our two-dimensional field of depth d, say, in the z-direction, $d\boldsymbol{S} = dx\hat{y}$ and $\boldsymbol{B} = \nabla \times [A(x, y)\hat{z}]$, so

$$2\mu W/d = \mu A_s I_s - \int_{-\infty}^{\infty} (AB_x)_{y=0}\, dx , \qquad (3.20)$$

where I_s is the total current in the current sheet and A_s is the value of the flux function on the sheet. We shall suppose without loss of generality that $A_s = 0$.

The corresponding expression to equation (3.20) for the energy W_0 due to a potential field [$\boldsymbol{B}_0 = \nabla \times (A_0 \hat{z})$] having the same normal field on $y = 0$ as $\boldsymbol{B}$ is

$$2\mu W_0/d = -\int_{-\infty}^{\infty} (AB_{0x})_{y=0}\, dx , \qquad (3.21)$$

since $A_0 = A$ on $y = 0$. Thus, subtracting equation (3.21) from (3.20) we obtain the free stored energy (W_f) as

$$2\mu W_f/d = \int_{-\infty}^{\infty} [A(B_{0x} - B_x)]_{y=0}\, dx . \qquad (3.22)$$

Now we write the field as

$$\boldsymbol{B} = \boldsymbol{B}_s + \boldsymbol{B}_{si} + \boldsymbol{B}_0 , \qquad (3.23)$$

where $\boldsymbol{B}_s$ is the field due to the current sheet, $\boldsymbol{B}_{si}$ due to its image and $\boldsymbol{B}_0$ the potential field due to the sources at $x = \pm a$ on the y-axis. Thus, on $y = 0$, $B_{sx} = B_{six}$, which is an even function of x, so equation (3.22) reduces to

$$2\mu W_f/d = -4 \int_0^{\infty} (AB_{sx})_{y=0}\, dx , \qquad (3.24)$$

where on $y = 0$ A vanishes for $0 \le x < a$ and equals $-\frac{1}{2}\pi B_0 (a^2 + h^2)^{1/2}$ for $x \ge a$.

The current in the sheet is μ^{-1} times the jump in B_y across it, namely from equation (3.16),

$$I(y) = \frac{2B_0 (h^2 - y^2)^{1/2} y}{\mu (y^2 + a^2)} . \qquad (3.25)$$

An element dy of the sheet at height y gives rise, according to the Biot-Savart Law, to a field of magnitude $B_s = \mu I\, dy/[2\pi(x^2 + y^2)^{1/2}]$ at a point on the x-axis of distance $(x^2 + y^2)^{1/2}$ from the element. This has an x-component $B_{sx} = B_s[y/(x^2 + y^2)^{1/2}]$, and so the resulting field due to the whole sheet is

$$B_{sx} = \frac{B_0}{\pi} \int_0^h \frac{(h^2 - y^2)^{1/2} y^2}{(y^2 + a^2)(x^2 + y^2)}\, dy . \qquad (3.26)$$

After substituting into equation (3.24), integrating over x, and putting $a^2 + h^2 = d^2$, we find

$$W_f = \frac{B_0^2 d^2}{\mu} \int_0^h \frac{(h^2 - y)^{1/2} y}{y^2 + a^2} \left(\frac{\pi}{2} - \tan^{-1} \frac{a}{y} \right) dy . \qquad (3.27)$$

This may be partly integrated analytically to give, finally,

$$W_f = \frac{B_0^2 d^3}{2\mu} \left[-\pi \left(\frac{h}{d} + \frac{1}{2} \log_e \frac{1 - h/d}{1 + h/d} \right) \right.$$
$$\left. -2 \int_0^{h/d} \frac{(h^2/d^2 - \bar{y}^2)^{1/2} \bar{y}}{\bar{y}^2 + a^2/d^2} \tan^{-1} \frac{a/d}{\bar{y}}\, d\bar{y} \right] , \qquad (3.28)$$

where $h^2/d^2 = 1 - a^2/d^2$.

Thus, our expression for the free energy (W_f) that is stored in the field and released during reconnection is of the form $B_0^2 d^3/(2\mu)$, which is the magnetic energy in a cube of side d, times a factor which depends on a/d alone. It is plotted, after evaluating equation (3.28) numerically, in Figure 6*c* for $B_0 =$ 10 G and for several values of the interaction distance d as a function of a/d. As a tends to zero, h tends to d and W_f has a logarithmic singularity, so we cut off the graphs at $a = 0.02d$. The energy in a 10 G field filling a cube of side $d = 2$ Mm, 5 Mm, 10 Mm, and 15 Mm, respectively, is 3×10^{18} J, 5×10^{19} J $= 5 \times 10^{26}$ ergs, 4×10^{20} J $= 4 \times 10^{27}$ ergs, 10^{21} J, respectively. Thus, the effect of the factor in equation (3.28) depending on a/d can be seen in Figure 6*d* to multiply $B_0^2 d^3/(2\mu)$ by factors of 4.4, 2.5, and 0.6 when $a/d = 0.1$, 0.2, and 0.5, respectively.

By comparison, the normal X-ray bright point emission is 10^{23}–10^{24} ergs s^{-1} (Golub et al. 1974) for typically 8 hr, making a total energy release of (3×10^{27})–(3×10^{28}) ergs (3×10^{20}–3×10^{21} J), so it can be seen that these values are of the same magnitude as those in Figure 6*c* when $d = 5$–10 Mm and $B_0 = 10$ G. If the corresponding magnetic field (B_0) and interaction distance (d) were different—for instance, B_0 being larger and d smaller—the energy would scale as $B_0^2 d^3$. It would be one of the main objects of a numerical experiment on flux interaction to estimate more accurately the energy release and another to study the regime of reconnection. It is also interesting to note that there is a wide range of lifetimes around the mean of 8 hr and consequently of the net energy release. Furthermore, during bright point flares, the peak emission is 10^{25}–10^{26} ergs s^{-1} for about 5 minutes, giving a total emission of 3×10^{27}–3×10^{28} ergs, the same as in an average 8 hr normal nonflaring bright point.

3.2. *Dynamic Reconnection at the X-Point*

So far in this section, we have presented a simple model for the quasi-static passive formation of a current sheet. In this section we extend the model to consider dynamic effects in response to motion of the sources at constant velocities. Titov & Priest (1993) and Priest, Titov, & Rickard (1993) have recently developed a self-consistent model for the time-dependent growth of a current sheet from a simple X-type field

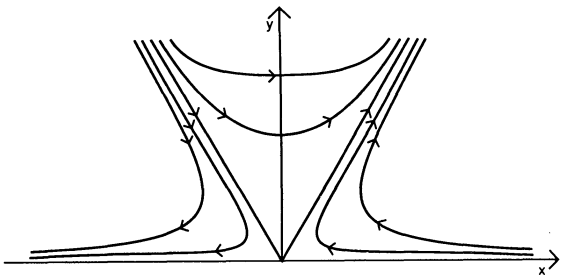

FIG. 7a

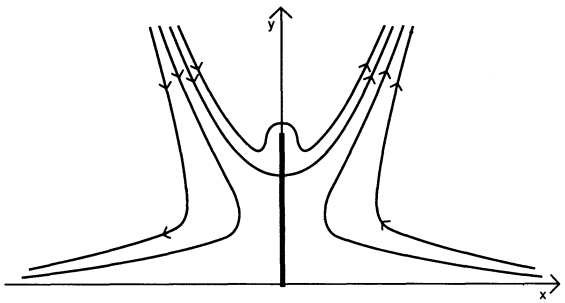

FIG. 7b

FIG. 7.—Magnetic field lines (*a*) close to the second-order null point and (*b*) during the dynamic growth of a current sheet from the null point.

($B_y + iB_x = z$). Here we adopt the same approach, in order to determine how a time-dependent current sheet may grow from our second-order null point given by equation (3.7). First, we change the variable from z to

$$Z^3 = -\frac{B_0}{3d^3} z^3 , \tag{3.29}$$

and so consider the initial field (Fig. 7*a*)

$$B_y + iB_x = 3iZ^2 , \tag{3.30}$$

with complex flux function

$$f = -iZ^3 . \tag{3.31}$$

We seek solutions of the equations of motion and induction,

$$\rho \frac{d\boldsymbol{v}}{dt} = \boldsymbol{j} \times \boldsymbol{B} , \quad \frac{\partial \boldsymbol{B}}{\partial t} = \nabla \times (\boldsymbol{v} \times \boldsymbol{B}) , \tag{3.32}$$

and expand in powers of the Alfvén Mach number ($\epsilon \ll 1$),

$$\boldsymbol{v} = \epsilon(\boldsymbol{v}_0 + \epsilon \boldsymbol{v}_1 + \cdots) , \quad \boldsymbol{B} = \boldsymbol{B}_0 + \epsilon \boldsymbol{B}_1 + \cdots . \tag{3.33}$$

To lowest order in our two-dimensional situation,

$$\boldsymbol{j}_0 = \boldsymbol{0} , \quad \frac{\partial \boldsymbol{B}_0}{\partial t} = \nabla \times (\boldsymbol{v} \times \boldsymbol{B}_0) , \tag{3.34}$$

so that we have an evolution through potential states which preserve the topology and so are accessible (Moffatt 1985) and need to be determined self-consistently.

To next order

$$\rho_0 \frac{d\boldsymbol{v}_0}{dt} = \boldsymbol{j}_1 \times \boldsymbol{B}_0 , \tag{3.35}$$

which implies an important constraint at lowest order, namely

$$\frac{d\boldsymbol{v}_0}{dt} \cdot \boldsymbol{B}_0 = 0 , \tag{3.36}$$

so that the acceleration is perpendicular to the magnetic field.

An elegant way of solving equations (3.35) and (3.36) is to write the magnetic field in terms of a flux function,

$$(B_x, B_y) = \left(\frac{\partial A}{\partial y}, -\frac{\partial A}{\partial x} \right) , \tag{3.37}$$

so that equation (3.35) becomes

$$\nabla^2 A = 0 , \quad \frac{dA}{dt} = 0 , \tag{3.38}$$

and also to introduce the conjugate harmonic function Φ. The aim then is to find the mappings $Z(f, t)$ and $f(Z, t)$ where

$$f = A + i\Phi . \tag{3.39}$$

Assuming that Φ is frozen to the plasma, the simplest way of satisfying equation (3.36) is by means of an acceleration-free flow

$$\frac{\partial^2 Z}{\partial t^2} = 0 , \tag{3.40}$$

with solution

$$Z = Z_0(f) + V_0(f)t , \tag{3.41}$$

where $Z_0(f)$ is the initial position and $V_0(f)$ the initial velocity.

Now, equation (3.31) gives the initial field, and so its inverse is

$$Z_0(f) = \frac{\sqrt{3} + i}{2} f^{1/3} . \tag{3.42}$$

If we assume an initial velocity

$$V_0(f) = -\frac{1}{4Z_0} , \tag{3.43}$$

equation (3.41) has solution

$$2Z_0 = Z + \sqrt{(Z^2 + t)} . \tag{3.44}$$

Since a plasma element preserves its value of f as it moves,

$$f = f_0 = -iZ_0^3 , \tag{3.45}$$

or, using equation (3.44),

$$f = -\frac{i}{8} [Z + \sqrt{(Z^2 + t)}]^3 , \tag{3.46}$$

which is our required solution for $f(Z, t)$.

The resulting field components are simply (Fig. 7*b*)

$$B_y + iB_x = -\frac{\partial f}{\partial Z} = -\frac{3i}{8} \frac{[Z + \sqrt{(Z^2 + t)}]^3}{\sqrt{(Z^2 + t)}} . \tag{3.47}$$

The corresponding flow components are

$$v_x + iv_y = \frac{\partial Z}{\partial t} = \frac{1}{Z_0} = \frac{2}{Z + \sqrt{(Z^2 + t)}} , \tag{3.48}$$

while the electric field is

$$E = \mathrm{Re}\,(vB) = -\mathrm{Re}\,\frac{3i[Z+\sqrt{(Z^2+t)}]^2}{16\sqrt{(Z^2+t)}}, \quad (3.49)$$

and the density is

$$\rho = \frac{\rho_0}{|\partial Z/\partial Z_0|^2} = \frac{\rho_0}{|1-4t/[Z+\sqrt{(Z^2+t)}]^2|}. \quad (3.50)$$

The solution has several interesting properties. Each plasma element moves with a constant velocity so that they converge on the y-axis and form a current sheet of length $2\sqrt{t}$. Although the form (3.47) is fairly simple, the corresponding expressions for $B_x(x, y, t)$, $B_y(x, y, t)$ are far from simple. The field and flow are of self-similar form with a similarity variable $Z/\sqrt{t}$. The top of the sheet moves up at a speed proportional to $t^{-1/2}$, swallowing up part of the magnetic flux in the process, while the remainder piles up around a region of reversed current and reversed curvature. The Poynting flux into the sheet grows in time, partly heating the plasma and partly accelerating particles. Also, the fact that field lines thread the current sheet allows particles and heat to escape into a much larger region than would otherwise be the case.

4. DISCUSSION: MORE GENERAL QUALITATIVE FEATURES

Here we discuss more general features of the basic model which has been presented above and raise many questions which we expect to be the subject of future developments in the theory and observations. In particular, we comment on the timing of the phenomena, variations from the basic model, the filament formation and eruption, flaring, and possible alternative configurations.

4.1. *Timing*

Bright points are observed to last on average 8 hr. In the simple form of our model (§§ 2 and 3), a bright point lasts for the duration

$$\tau_I = \frac{d}{V_0} \quad (4.1)$$

of the interaction phase, where $d = [2f/(\pi B_0)]$ is the interaction distance (minus the fragment width) and $2V_0(\equiv -2\dot{a})$ is the relative speed of approach of the magnetic fragments. Adopting typical values for d and V_0 of 9 Mm and 0.3 km s^{-1}, respectively, we obtain a bright-point lifetime of 3×10^4 s or 8 hr, as required. Much briefer BPs with lifetimes of only a few minutes may represent tiny flares due to impulsive reconnection in a BP that is too faint to be easily observed.

The duration of the cancellation phase is

$$\tau_c = \frac{w}{V_0}, \quad (4.2)$$

where w is the width of a fragment. Thus, adopting typical values for w and V_0 of 1–5 Mm and 0.3 km s^{-1} for intracell/intracell cancellations, we obtain a duration for cancellation of 1–5 hr, as required (observation 3c). Taking w = 1–10 Mm and V_0 = 0.3–0.1 km s^{-1} instead for network/network or ephemeral region/network cancellations, we find a lifetime of 1–30 hr, again as required. Wider fragments or slower approach speeds would yield longer durations. The observed time for tiny filament formation and eruption is about an hour or two and so is consistent with the above estimate, since it is less than τ_c and the formation and eruption in the simple model occurs during cancellation.

Bright points are observed to continue into the cancellation phase (Webb et al. 1993), but it is not yet known for how long, because of the limited duration of the rocket flights. Some BPs are seen to occur during cancellation and some before, and also there are many CMFs with no BP. Is this because some never have BPs or because BPs last for only part of the cancellation phase? Also, the associations of BPs with CMFs and ERs may well vary with the solar cycle, which could explain some of the differences between the *Skylab* and rocket data (Golub et al. 1989; Webb et al. 1993).

4.2. *Variations in the Basic Model*

There are several possible variations on the theme of the basic model we have presented. For example, in Figure 2 we have assumed that the overlying field has a strong component in a direction perpendicular to the plane of the figure. We did this mainly because, as the fragments approach one another, the overlying chromosphere has no Hα fibrils joining the two fragments (observation 1a), since the chromospheric channel in Figure 2(i) has its main field component perpendicular to the line of approach. When viewed from above, this produces the structures shown in Figure 3*a*. If, as is less likely, the strong component out of the plane only exists for the overlying field and not the magnetic fragments, then the region near the separatrix in Figure 2 would be one of large shear or even a current sheet.

We have shown the overlying field in Figure 2 to have a component in the plane. According to Martin (1986), there are usually no ordinary fibrils connecting the poles during the cancellation phase, although tiny flare loops can connect the opposite polarities and sometimes be observed in absorption as they cool. However, a long time before this phase in the preinteraction phase one does sometimes observe such fibrils—e.g., on page 880 of Harvey (1985) they are present at 20.14, well before the cancellation at 22.22. In such a case, one suggestion is that the fibrils do not really magnetically connect the fragments but instead are present in the overlying field lines of Figure 2(i). The overlying field may in theory be inclined at any angle to the line joining the two fragments. Also, when apparent connecting features are occasionally seen, they do not resemble normal fibrils and do not persist for hours; another possibility is that they are cooled flare loops or field lines that have reconnected and are now joining the poles. K. Harvey has several good examples of fibrils connecting poles during cancellation, and clearly it is important to study this aspect in detail in the future.

Another variant which we mentioned in § 5.1 concerns the location of the reconnection during the cancellation phase. Our view is that the most likely location is in or close to the photosphere itself for three reasons, namely:

(1) the fact that there are usually no ordinary fibrils connecting the poles during cancellation (observation 1a);

(2) that reconnection may be easier there because the classical magnetic diffusivity (η) scales with temperature T as $T^{-3/2}$ and so has its greatest value at the temperature minimum;

(3) that photospheric reconnection transfers magnetic flux and energy to the corona, where it may be stored and subsequently erupt, as indicated by tiny erupting filaments.

The second reason is not clinching, since, if you vary the diffusivity in standard models of nonlinear steady reconnection, the main effect is a change of scale of the reconnection region rather than a change of reconnection rate. The first reason could also be satisfied if the reconnection current sheet were large and extended from the photosphere to the chromosphere or if the reconnection point were located in the chromosphere and the plasma on field lines below the X-point do not show up as fibrils because it is not dense enough. This possibility of chromospheric reconnection we have referred to in our preliminary thoughts on the problem as *reconnection submergence* (Priest 1992), since the field lines reconnect at a point above the photosphere and then submerge below it after they are reconnected. It should also be noted that the height of the magnetograms is not known precisely: the magnetic fields are measured in the wings of the line and so probably slightly above but very close to the photosphere.

4.3. *Filament Formation and Eruption*

The study by Hermans & Martin (1986) of tiny filaments sometimes forming and erupting during the cancellation phase is very interesting and deserves much more study. They observed 61 such filaments, which usually resemble a fibril and sometimes a loop, and conservatively estimated that at least 600 would occur on the Sun per day. One of them is shown in Figure 8 (Plate 10). Their lengths and lifetimes range between 4–40 Mm and 15–201 minutes, respectively, with mean values of 11 Mm and 70 minutes. The length of the eruptive phase varies between 6 and 77 minutes, with an average of 26 minutes. Seventy-five percent of them are associated with very small flares, and 75% are associated with conspicuous cancelling magnetic features. The remainder were probably associated with fields below the detection limit on the magnetograph. The filament appears after cancellation has begun. Sometimes a filament lies along the division between polarities, and sometimes one or both ends of the filament terminate near the division. Some of the features called macrospicules by Moore et al. (1977) and LaBonte (1979) appear to be the same type of features that Hermans & Martin (1986) identified as small-scale erupting filaments.

Figure 3 shows how a tiny filament may naturally form along the field during cancellation. As seen from above (Figs. 3*a* and 3*b*) or the side (Fig. 3*c*), field lines from the magnetic fragment reconnect and form a long field line full of dense plasma, which naturally rises and threads between the fragments viewed from above (in a way that has been proposed for normal-sized filaments by Van Ballegooijen & Martens 1989). If the field lines from one fragment are initially short, the filament may end near the CMF, as sometimes observed (Fig. 3*b*). Alternatively, a short filament may occur in a plasmoid formed and naturally erupting in the initial stages of cancellation.

Normal quiescent prominences are widely thought to form in a very slight dip in the magnetic field (e.g., Kippenhahn & Schluter 1957; Priest 1989; Ruzdjak & Tandberg-Hanssen 1990) and to have the magnetic field in them horizontal and inclined at about 20 degrees to the prominence axis (Leroy 1989). However, fine-scale structure is observed to be inclined at roughly the same angle and so perhaps to be aligned locally along the field, and some authors have suggested that at least some filaments may instead be oriented along a flux tube (Kuperus & Raadu 1974; Hood & Priest 1979; Priest, Hood, & Anzer et al. 1989). One wonders, therefore, what is the orientation of our tiny filaments relative to the field: we are suggesting here that they form along the field. (In fact, the configuration that we are proposing here may well give a reasonable model at a much larger scale for a typical large filament channel and, once the large filament has formed, for the field around the filament itself.)

Normally, the canceling magnetic fragments appear to undergo direct head-on collisions at resolutions of 2″–4″. For instance, network/network collisions are constrained to follow the supergranule boundary. However, intracell/intracell collisions have a greater chance of a glancing collision. For cases in which they are not head-on, another way in principle of creating a filament would be to have the field below the X-point in the interaction phase (Fig. 2[iii]) having a large component out of the plane and being highly sheared and twisted. When the field is sheared enough, a filament may form and then erupt.

A model for the way a normal filament in a magnetic arcade evolves slowly through a series of equilibria and then reaches a point of nonequilibrium or catastrophe and erupts was proposed by Priest & Forbes (1990), developed by Forbes & Isenberg (1991), and studied with a numerical experiment by Forbes (1990, 1991). This is based on the earlier model of Van Tend & Kuperus (1978), Kuin & Martens (1986), and Martens (1986) and uses flux cancellation to drive the slow evolution (Van Ballegooijen & Martens 1989) toward nonequilibrium, but it does not use circuit equations since we believe them to provide a misleading modeling of the MHD process. Here we follow the spirit of the Priest-Forbes model and consider briefly whether the same scenario can work for a tiny filament of strength I at height h suspended above a pair of equal and opposite magnetic fragments of flux $\pm f$ at locations $z = \pm a$, where $z = x + iy$, and having an image current $(-I)$ a distance h below the photosphere.

The resulting magnetic field components have the form

$$B_y + iB_x = \frac{I}{z - ih} - \frac{I}{z + ih} + \frac{if/\pi}{z - a} - \frac{if/\pi}{z + a}, \tag{4.3}$$

or

$$B_y + iB_x = \frac{2i[(Ih + fa/\pi)z^2 + (fh/\pi - Ia)ah]}{(z^2 + h^2)(z^2 - a^2)}. \tag{4.4}$$

Now the magnetic force acting on the filament is

$$\frac{2\pi I}{\mu}\left(-\frac{I}{2ih} + \frac{2ifa/\pi}{-h^2 - a^2}\right),$$

where the term in brackets is the magnetic field at the filament due to the image current and the two magnetic fragments. For the filament to be in equilibrium (neglecting gravity), this force must vanish, and so

$$h^2 - \frac{4fa}{\pi I}h + a^2 = 0. \tag{4.5}$$

This has two solutions, and we suppose the filament is in equilibrium on the lower branch,

$$h = \frac{2fa}{\pi I} - \left(\frac{4f^2}{\pi^2 I^2} - 1\right)^{1/2} a, \tag{4.6}$$

so that the height (h) lowers as a decreases, or the current I increases and h increases as the flux decreases. Eventually, a

1994ApJ...427..459P